coatings

Article

High-Temperature Oxidation Resistance and Tribological Properties of Al_2O_3/ta-C Coating

Asad Alamgir [1,*], Andrei Bogatov [1], Taivo Jõgiaas [2], Mart Viljus [1], Taavi Raadik [3], Jakob Kübarsepp [1], Fjodor Sergejev [1], Andreas Lümkemann [4], Jan Kluson [5] and Vitali Podgursky [1]

1 Department of Mechanical and Industrial Engineering, Tallinn University of Technology, Ehitajate tee 5, 19086 Tallinn, Estonia; andrei.bogatov@mail.ru (A.B.); mart.viljus@taltech.ee (M.V.); jakob.kubarsepp@taltech.ee (J.K.); fjodor.sergejev@taltech.ee (F.S.); vitali.podgurski@taltech.ee (V.P.)
2 Institute of Physic, University of Tartu, W. Ostwaldi 1, 50411 Tartu, Estonia; taivo.jogiaas@ut.ee
3 Department of Materials and Environmental Technology, Tallinn University of Technology, Ehitajate tee 5, 19086 Tallinn, Estonia; taavi.raadik@taltech.ee
4 PLATIT AG, Eichholzstrasse 9, CH-2545 Selzach, Switzerland; a.luemkemann@platit.com
5 PLATIT A.S., Prumyslova 3020/3, CZ-787 01 Sumperk, Czech Republic; j.kluson@platit.com
* Correspondence: asadalamgir.shaikh@live.com

Abstract: The focus is on the oxidation resistance and tribological performance of ta-C and Al_2O_3/ta-C coatings. The wear tests were carried out on the ball on disc tribometer at room (25 °C) and high (400, 450 and 500 °C) temperatures in ambient air with Si_3N_4 balls as counterbodies. Scanning electron microscopy and Raman spectroscopy were used to analyze the surface morphology and chemical bonding, respectively. The Al_2O_3/ta-C coating exhibited better oxidation resistance and tribological performance at elevated temperatures than the ta-C coating. The Raman analysis revealed that a thin alumina layer suppresses structural changes in the ta-C coating at elevated temperatures, thus preserving the sp^3 content.

Keywords: ta-C coating; oxidation resistance; tribology; high temperature

Citation: Alamgir, A.; Bogatov, A.; Jõgiaas, T.; Viljus, M.; Raadik, T.; Kübarsepp, J.; Sergejev, F.; Lümkemann, A.; Kluson, J.; Podgursky, V. High-Temperature Oxidation Resistance and Tribological Properties of Al_2O_3/ta-C Coating. *Coatings* **2022**, *12*, 547. https://doi.org/10.3390/coatings12040547

Academic Editor: Shijie Wang

Received: 10 March 2022
Accepted: 15 April 2022
Published: 18 April 2022

1. Introduction

It is estimated that one-fourth of the energy consumption in the world originates from tribological phenomena [1]. Friction and wear lead to an increase in energy consumption and material losses that cause huge economic and environmental impact. Exploitation of mechanical systems under high friction contact conditions as well as replacement of worn parts require large amounts of energy and materials. Therefore, minimization of heat generation, friction and wear is a key factor for sustainable development of the global economy. Wear-resistant low friction coatings play a crucial role in the modern surface engineering [2,3].

In the past few decades, the development of the diamond like coating (DLC) has become a research hotspot due to its low coefficient of friction (COF), high hardness, excellent biocompatibility and chemical inertness [3–5]. Amorphous carbon coatings can be divided into two categories, i.e., hydrogenated (hydrogenated DLC (a-C:H), hydrogenated tetrahedral amorphous carbon (ta-C:H), etc.) and non-hydrogenated (hydrogen free DLC (a-C), tetrahedral amorphous carbon (ta-C), etc.) coatings [3,6]. Tribological properties of hydrogenated coatings differ from those of non-hydrogenated due to hydrogen content and chemical bonding [2,7]. Relatively thick hydrogenated DLC coatings can be prepared, which provide a good mechanical barrier, however, these coatings can be vulnerable to water environment [8]. Hydrogen free DLC coatings are less sensitive to water environment, however, the high residual stress limits their application [9]. According to Ronkainen et al. [2], ta-C has higher wear resistance than the a-C:H coating. The superior mechanical properties of ta-C coatings are mainly due to the presence of higher amount of strong covalent bonds (sp^3) between the carbon atoms [3,10,11].

Friction and wear of DLC and ta-C coatings at high temperatures (HT) depend on the chemical structure of coatings, substrate material, contact pressure, operating temperature, and the environment [12,13]. The sp^2/sp^3 ratio is a key factor affecting mechanical and tribological properties of amorphous carbon coatings [2,3,10]. The value of sp^2/sp^3 ratio depends mainly on the deposition method [13]. The DLC coatings undergo oxidation, graphitization, dehydrogenation and lose their lubricating ability in the sliding tests at HT in air [14]. In addition to environmental conditions, the surface modification is induced by tribo-chemical reactions within the contact area, which influences strongly the wear mechanisms [15]. The graphitization of DLC at elevated temperatures (200–300 °C) causes degradation of hardness [16–18]. On the other hand, the non-hydrogenated ta-C coatings are more stable at HT (400–450 °C) owing to higher sp^3 bonds fraction [19,20]. However, the oxidation resistance of ta-C coatings deposited onto the surface of moving parts is still too low at HT under external forces. According to Deng et al. [19], the ta-C coating is easily peeled off at temperatures higher than 450 °C in ambient air. A more thorough discussion of the tribological behavior of the DLC and ta-C coatings at HT can be found in our recent publication [21].

An alternative approach to reduce the wear at extreme conditions includes the preparation of an adaptive top layer (for details see Refs. [21,22]). It was shown in our previous studies on nanocrystalline diamond (NCD) and a-C:H:Si coatings coated with the thin Al_2O_3 layer that the alumina layer acts as an adaptive layer [21–23]. The increasing of wear scar width and therefore decreasing of contact pressure were observed in the sliding tests at room temperature (RT).

In the present study, tribological properties of the ta-C and Al_2O_3/ta-C coatings were analyzed to compare the oxidation resistance in the sliding tests at HT in air. According to our earlier findings, high contact pressure between the counterbodies results in breaking the thin Al_2O_3 layer during the early stages of running-in period and it acts as the adaptive layer [21,22]. The present study is intended to give further insight into the influence of the thin alumina layer on the tribological behavior of carbon-based coatings at HT. The studies on the NCD and a-C:H:Si coatings revealed that the thin alumina layer can improve tribological performance at HT [21,22].

2. Materials and Methods

The 1 μm thick ta-C coating was deposited onto WC-Co substrates (Ø 13 mm, height 5 mm, Ra = 0.05 μm) using LACS-technology (Lateral Arc with Central Sputtering) Pi411 PVD deposition system (PLATIT®, Grenchen, Switzerland) [24]. Prior to the deposition, the substrates were rinsed with alcohol and placed into sample holders in the deposition chamber. The coating process starts with Ar and metal ion etchings, followed by the deposition of Cr/CrC adhesion layer, using arc evaporation of Cr and C sputtering at the same time at 150 °C. The hardness of the ta-C coating was 50 GPa [25]. The atomic layer deposition (ALD) technique was used to deposit the 200 nm thin Al_2O_3 film on top of ta-C layer. The deposition was carried out in a flow type reactor (Picosun R200, Espoo, Finland) at 300 °C, with trimethylaluminum (TMA, $Al_2(CH_3)_6$), nitrogen as the purge gas and water as a precursor were used. The pressure was maintained at 10 mbar (1 kPa). The precursor pulse lengths were 0.1/4/0.1/10 s for TMA/N_2/H_2O/N_2, respectively. After 2000 cycles, the Al_2O_3 film was 200 nm thick. The film thickness was measured by a spectroscopic ellipsometer (SemilabSopraGES-5E, Budapest, Hungary), using 365 and 633 nm wavelengths at an angle of 75° on Si(100) reference substrates. The Cauchy approximation was used to fit the data [21,22]. Thin amorphous alumina layer had hardness 10 GPa [26].

The tribological behavior of the coatings were studied using a ball-on-disk type tribometer (Bruker® UMT-2, Billerica, MA, USA) equipped with a high-temperature chamber with rotary drive. The Si_3N_4 ball with Ø 10 mm was used as counterbody. The ball has a hardness of 1400–1700 HV, a Young's modulus of 310 GPa, and a Poisson ratio of 0.27.

Wear tests were conducted on each type of coatings, i.e., ta-C and Al_2O_3/ta-C, at RT, 400, 450, and 500 °C. The normal load was 2 N, the speed of rotation 200 RPM and the wear

track diameter was 3 mm. The heating rate prior to the HT sliding tests was 5 °C/min with the temperature stabilization period for 45 min. The duration of the sliding tests was either 10 or 180 min. The relative humidity was 45 ± 5%. The stylus profilometry (Mahr Perthometer®, Göttingen, Germany) was used to investigate the depth, width and shape of wear scars. The averaged line scan was obtained by taking five-line scans across each wear scar. The apparent volume (V) of wear scar was calculated using formula $V = S \times l$, where S is the cross-section area and l is the wear scar length. Each type of wear tests was conducted three times to estimate the averaged value of wear volume.

Micro-Raman spectroscopy and scanning electron microscopy (SEM) were used to examine the chemical structure and morphology of the pristine and wear scar surfaces. The Renishaw inVia micro-Raman (Renishaw, New Milles, UK) setup equipped with an Ar^+ ion laser (514 nm wavelength) was used to perform the micro-Raman measurements. The SEM images were investigated by the (Zeiss EVO® MA-15 system, Oberkochen, Germany) with LaB6 cathode in secondary electron mode, applying an accelerating voltage of 10–15 kV and at 6.5–8.5 mm working distance.

3. Results and Discussion

Figure 1 shows the surface morphology of as-deposited ta-C and Al_2O_3/ta-C coatings. The alumina layer grows conformally, resembling the morphology of the ta-C surface [21,22]. The roughness Ra of ta-C and Al_2O_3/ta-C was 0.08 and 0.09 µm, respectively. The droplets and pores are visible on the surface of both coatings.

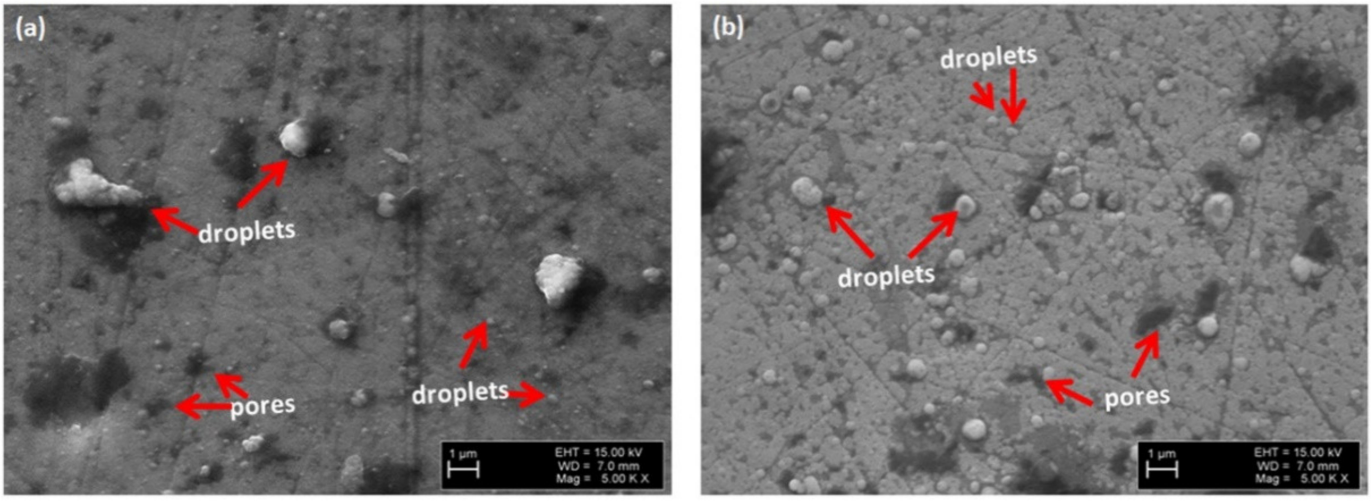

Figure 1. SEM images of the pristine surface of (**a**) ta-C and (**b**) Al_2O_3/ta-C coatings.

Figure 2 shows COF versus cycle curves after the sliding tests at RT and HT against Si_3N_4 balls. The COF behavior of the ta-C coating at RT test indicates the running-in period up to 3000 cycles long, which is followed by a period, and afterwards from 7000 and 22,000 cycles with a number of spikes in the COF curve. Finally, the COF value stabilized at about 0.05. In contrast, for the Al_2O_3/ta-C coating, a very short running-in period is followed by a continuous decrease of COF value up to 0.03. In the case of sliding at HT, very short running-in periods were observed for both ta-C and Al_2O_3/ta-C coatings. The COF value changes from 0.01 to 0.08 in the test at 400 °C for the ta-C coating, while COF starts to rise after 12,000 cycles of sliding. A stable sliding regime was observed for the Al_2O_3/ta-C coating with the COF value between 0.01–0.06 up to 17,000 cycles. Finally, COF increases, and coating wears out after 34,000 cycles of sliding. The COF value increases gradually from 0.05 to 0.3–0.55 in the test at 450 °C for the ta-C coating; a significant noise indicates that the coating starts to fail after 2000 cycles of sliding. In the test at 500 °C, the ta-C coating failed at the early stage of sliding. However, in the case of Al_2O_3/ta-C coating in the test at 450 °C, the COF value remained stable up to 32,000 cycles of sliding,

and the coating survived up to 13,000 cycles in the test at 500 °C. These results prove a protection ability of the thin alumina layer, which protects the underlying ta-C layer against the oxidation attack at HT.

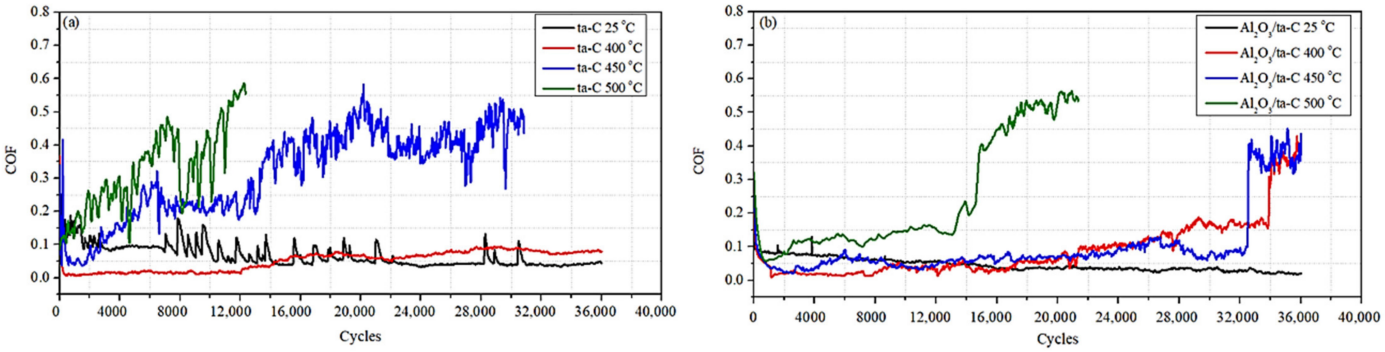

Figure 2. COF versus cycles curves taken on the (**a**) ta-C and (**b**) Al_2O_3/ta-C coatings at different temperatures.

Figure 3 shows the depth profiles of wear scars observed on the ta-C and Al_2O_3/ta-C coatings after the sliding tests for 10 and 180 min at RT. The width of the wear scars for the ta-C coating was approximately 160 and 260 μm and the depth of 0.18 and 0.3 μm, respectively (Figure 3a,b). Similarly, the width and depth of the wear scars for the Al_2O_3/ta-C coating were approximately 290 and 380 μm and 0.3 to 0.4 μm, respectively. The thickness of alumina layer was 0.2 μm (Figure 3c,d). The increase in the width of the wear scars of Al_2O_3/ta-C demonstrates the adaptation effect, i.e., an increase in the contact area leads to a decrease in the contact pressure. The wear scar width is larger for the Al_2O_3/ta-C coating after the tests for 180 min, i.e., the initial period of sliding determines the tribological behavior during the subsequent stages of sliding (hereditary effect). The depths of wear scars within the ta-C layer on the ta-C and Al_2O_3/ta-C coatings after the sliding tests for 180 min were approximately 0.3 and 0.1–0.2 μm, respectively. In conclusion, the thin alumina layer reduces the wear of the ta-C layer in the case of Al_2O_3/ta-C, in comparison with the ta-C coating, while the frictional behavior at RT is similar (Figure 2). Similar findings were reported in studies on the Al_2O_3/NCD and Al_2O_3/a-C:H:Si coatings as well [21,22].

The depth profiles of wear scars observed on both types of coatings after the sliding tests at HT (400–500 °C) are shown in Figure 4. The shorter (10 min) tests were carried out to investigate the tribological properties of coatings prior to coating failure. In the case of ta-C coating, the depth of wear scars increases quickly with the temperature increasing (Figures 3a and 4a–c). In the case of Al_2O_3/ta-C, an increase in depth and width can be seen as well (Figures 3c and 4d–f), and the width after the tests at highest temperatures (450 and 500 °C) is about twice larger than with the ta-C coating (Figure 4b,c,e,f). The depth of the wear scars (within ta-C layer) after 10 min friction tests at RT, 400, 450 and 500 °C is about 0.18, 0.45, 0.7 and 0.75 μm for ta-C and 0.1, 0.15, 0.3 and 0.3 μm for Al_2O_3/ta-C coating. Thus, the different shapes of the wear scars reflect a dissimilarity of wear mechanisms of ta-C layer for the ta-C and Al_2O_3/ta-C coatings, and a longer operational lifetime can be expected for Al_2O_3/ta-C in contrast to the ta-C coating under HT conditions in air. In other words, the adaptation effect and chemical conditions within the wear scar can influence the tribological behavior.

Figure 5 shows SEM images of the wear scars observed on the ta-C and Al_2O_3/ta-C coatings after the RT and HT sliding tests. The annealing defects appear on the ta-C surface during the sliding tests. In the case of ta-C coating (Figure 5a–d), the concentration of defects increases with the temperature of the sliding test, particularly after the tests at 450 and 500 °C. Probably, more intensive oxidation occurs at the ta-C coating surface at higher temperatures, in comparison with the Al_2O_3/ta-C coating (Figure 5e–h).

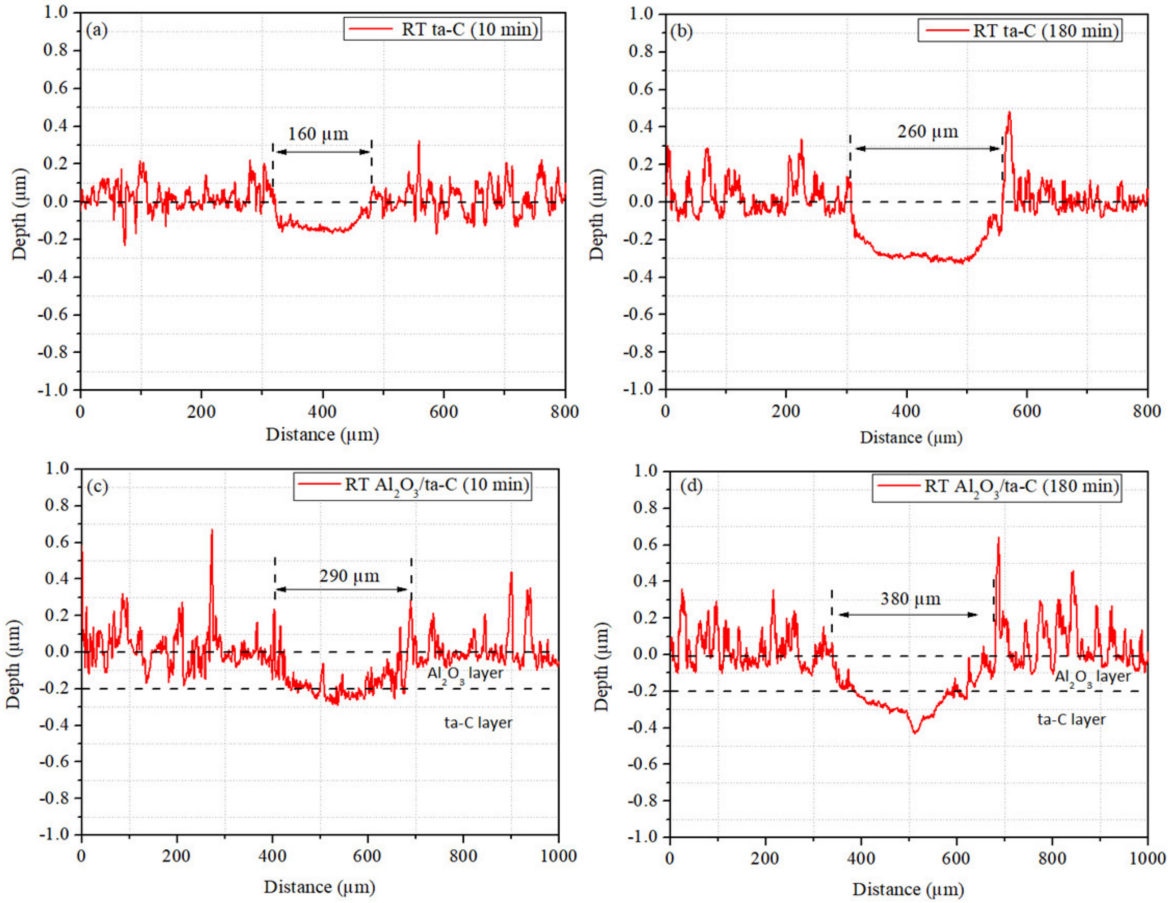

Figure 3. Depth profiles of wear scars observed on the ta-C and Al_2O_3/ta-C coatings after the sliding tests for (**a**,**c**) 10 min and (**b**,**d**) 180 min at RT.

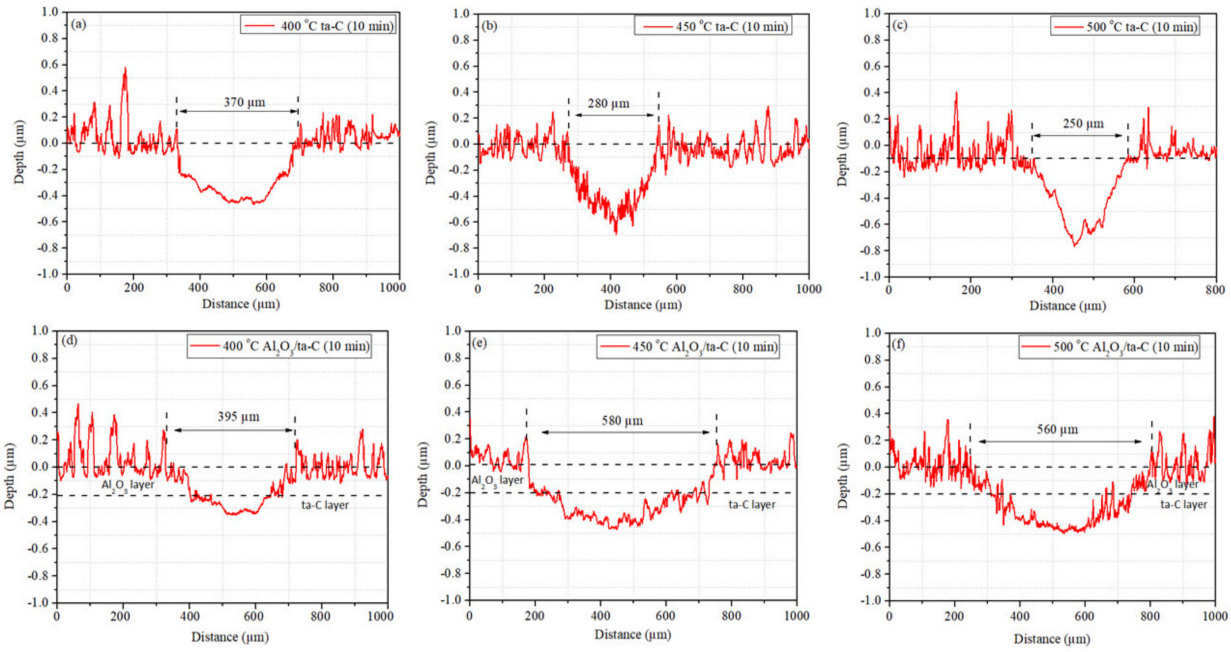

Figure 4. Depth profiles of wear scars observed on the (**a**–**c**) ta-C and (**d**–**f**) Al_2O_3/ta-C coatings after the sliding tests for 10 min at 400, 450 and 500 °C.

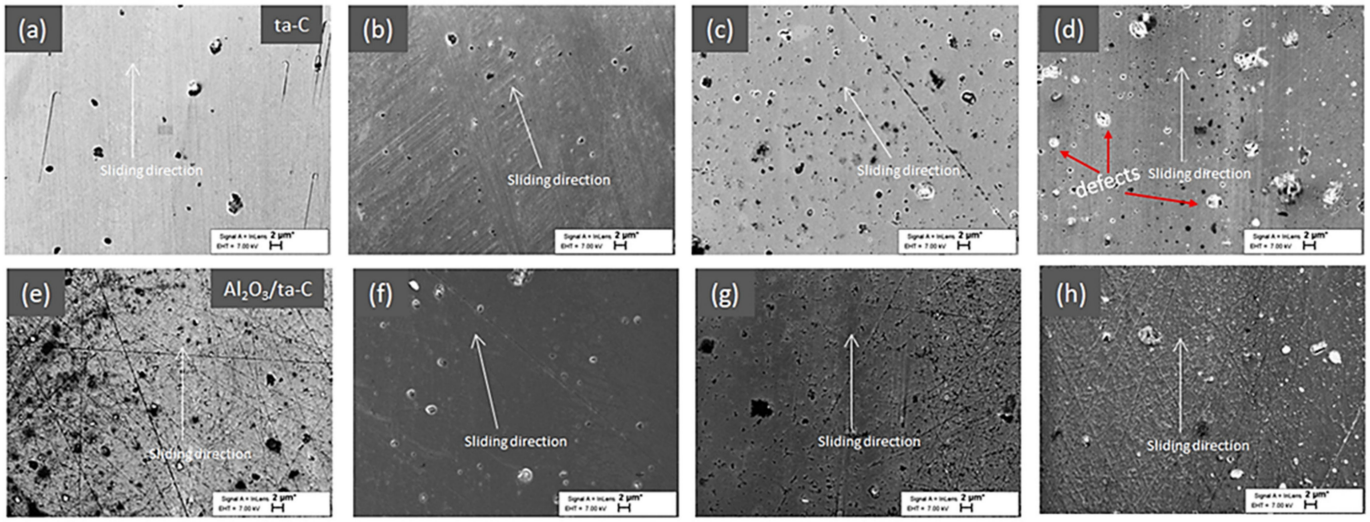

Figure 5. SEM images of the wear scars after tribological tests for 10 min at (**a**,**e**) RT, (**b**,**f**) 400 °C, (**c**,**g**) 450 °C and (**d**,**h**) 500 °C on both types of coatings.

Figure 6 shows the apparent wear volumes of the ta-C and Al_2O_3/ta-C coatings measured after the sliding tests. The wear volume loss of the Al_2O_3/ta-C coating is the sum of the wear volumes of alumina and ta-C layers (Figures 3 and 4). The black color indicates the wear volume loss of the ta-C layer, and the red color indicates the wear loss of the thin alumina layer. The wear volume loss of the ta-C layer is higher for the ta-C coating as compared with the Al_2O_3/ta-C coating for all testing regimes.

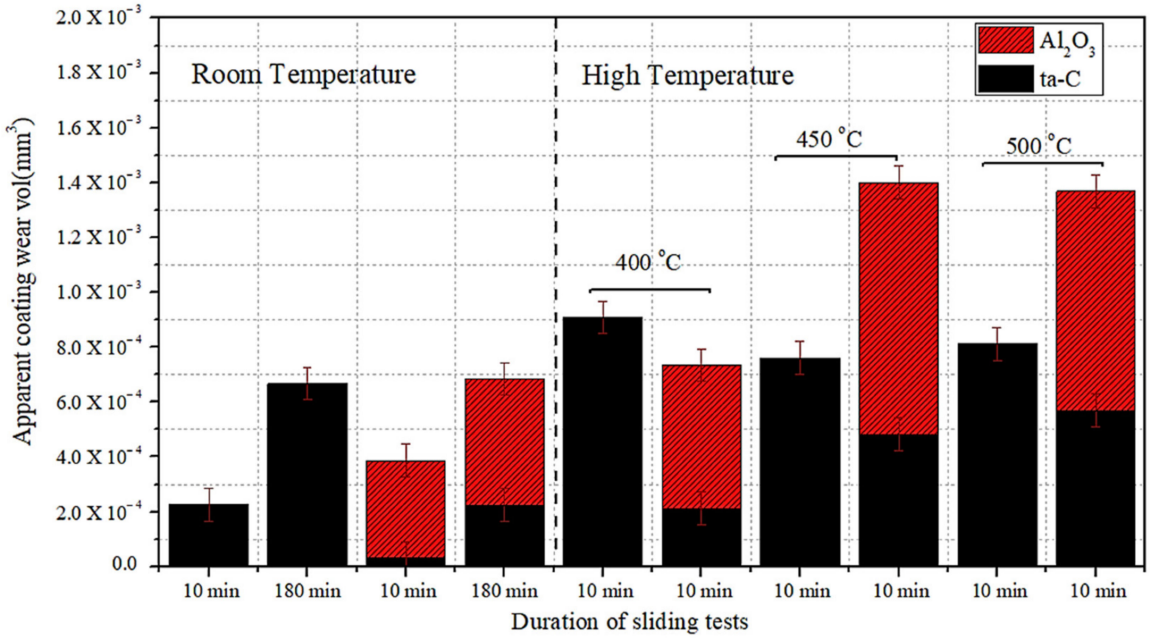

Figure 6. Apparent wear volumes on the ta-C (black) and Al_2O_3/ta-C (black + red) coatings.

Raman spectroscopy is a standard technique to reveal the nature of carbon–carbon bonding [27–29]. Raman measurements were repeated for at least three different locations within the wear scar. The results obtained on the pristine and wear scar surfaces of the ta-C and Al_2O_3/ta-C coatings are shown in Figures 7 and 8. The D and G band peaks position and intensity and full width at half maximum of the G peak (FWHM(G)) were obtained using Gaussian functions fitting of Raman spectra. The G peak is assigned to the stretching of sp^2 bonds on both ring and chains, whereas the D peak is assigned to the breathing

mode of sp^2 bonds in rings [30]. The t-Pa peak at 1054 cm^{-1} corresponds to the vibrational modes in trans-polyacetylene [31]. The relative content of sp^2 to sp^3 bonds is related to the D and G peaks intensity ratio [30]. The Raman G peak (1548–1557 cm^{-1}) was observed in spectra taken on the pristine and wear scar surfaces of both coatings (Figures 7 and 8). The G band peak shifts to higher value (1576 cm^{-1}) after the sliding tests at 500 °C for the ta-C coating (Figure 7d), which indicates changes in the structure of the sp^2 bonds. On the other hand, the Al_2O_3/ta-C coatings shows no significant G peak shift within the wear scar after HT sliding tests (Figure 8b–d). Similar behavior of the G peak was observed in our previous study on the a-C:H:Si and Al_2O_3/a-C:H:Si coatings [21].

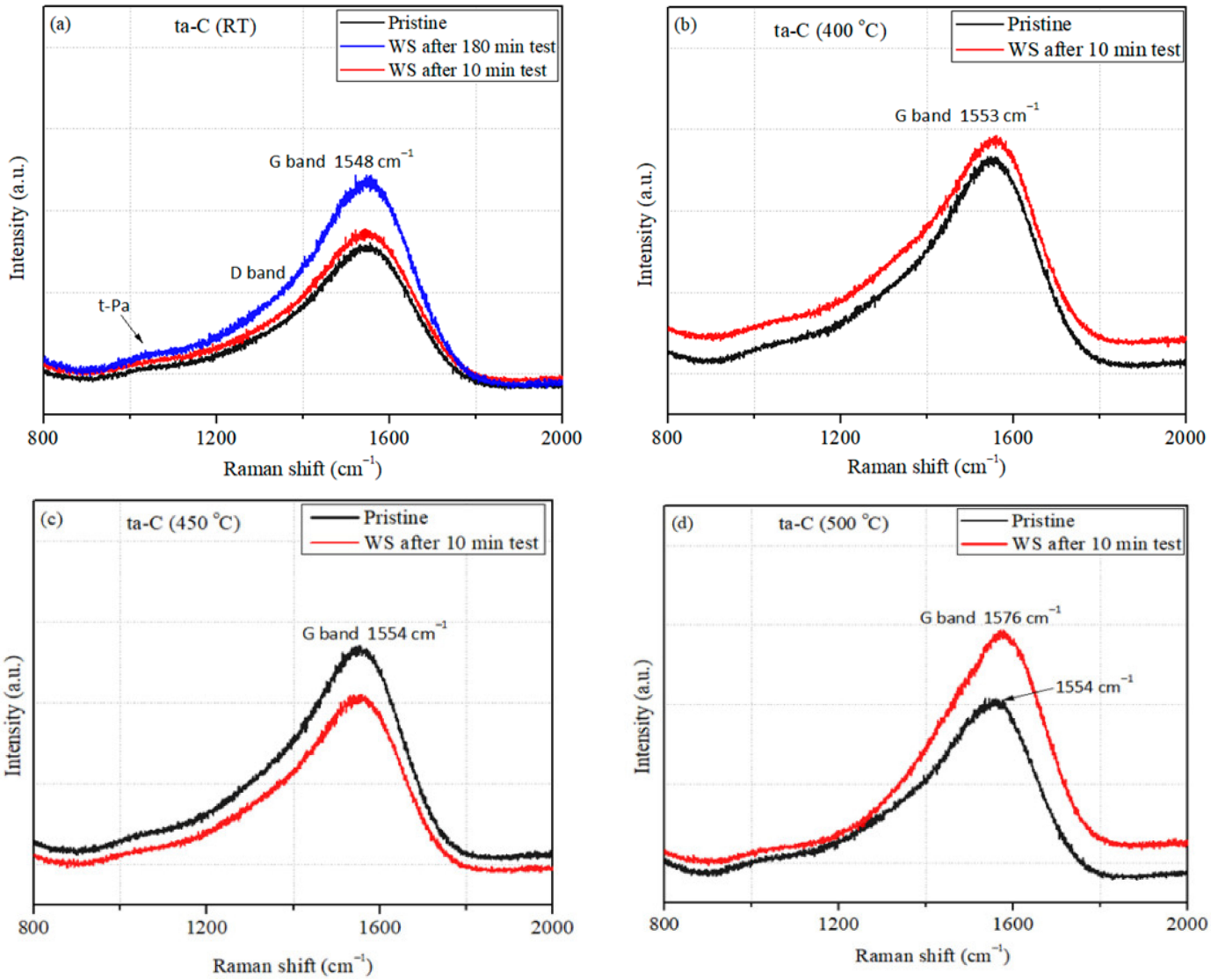

Figure 7. Raman spectra taken on the pristine and within wear scar surfaces of the ta-C coating after the sliding tests at (**a**) RT, (**b**) 400 °C, (**c**) 450 °C and (**d**) 500 °C.

The I_D/I_G ratio and FWHM(G) extracted from Raman spectra taken within the wear scars are shown in Figure 9. The smaller value of the I_D/I_G ratio corresponds to the higher sp^3 bonds fraction and therefore higher coating hardness. It is expected that the Al_2O_3/ta-C coating possesses better mechanical properties at HT as compared with the ta-C coating due to higher sp^3 bonds fraction (Figure 9a). The FWHM(G) value for DLC is sensitive to the stress-related disorder in the sp^2 carbon clusters [32]. Casiraghi et al. [33] suggest that FWHM(G) quantifies the bond length and angle disorder in sp^2 clusters. The size of sp^2 clusters within the sp^3 network decreases as the sp^3 content increases, thus sp^2

clusters become more strained. For instance, FWHM(G) increases with the increase of the sp^3 bonds content in the H-free DLC [33–35]. The larger width of the G peak observed for Al_2O_3/ta-C after the sliding tests at HT indicates smaller sp^2 fraction and higher stress within the sp^2 clusters in Al_2O_3/ta-C as compared with the ta-C coating (Figure 9b). The abovementioned shift of the Raman G peak to higher value in the tests at 500 °C observed on the ta-C coating is in a good agreement with this conclusion, i.e., it indicates structural changes within the sp^2 carbon clusters as well. The analysis of both the I_D/I_G ratio and FWHM(G) suggests that the content of sp^3 bonds is higher for the Al_2O_3/ta-C coating in contrast to the ta-C one after the sliding tests at HT. Therefore, enhanced tribological properties (higher hardness and thermal stability) of the Al_2O_3/ta-C coating at HT can be related with the higher content of the sp^3 bonds in the wear scar area as compared with the ta-C coating. A similar conclusion was reached in the case of Al_2O_3/a-C:H:Si [21] and DLC doped with oxygen [36,37] tested at HT in air. In addition, the duration of extended tests was 180 min, i.e., the entire surface of the ta-C coating was exposed to air at HT during the sliding tests. Therefore, the ta-C coating surface was oxidized and the crystal structure of the top and deeper layers of the ta-C coating was changed, leading to the fast increase of the wear scar depth observed in HT tests (Figure 4a–c). It was shown in our study on the Al_2O_3/NCD coating [22] that the alumina layer is the atmospheric oxygen diffusion barrier layer as well.

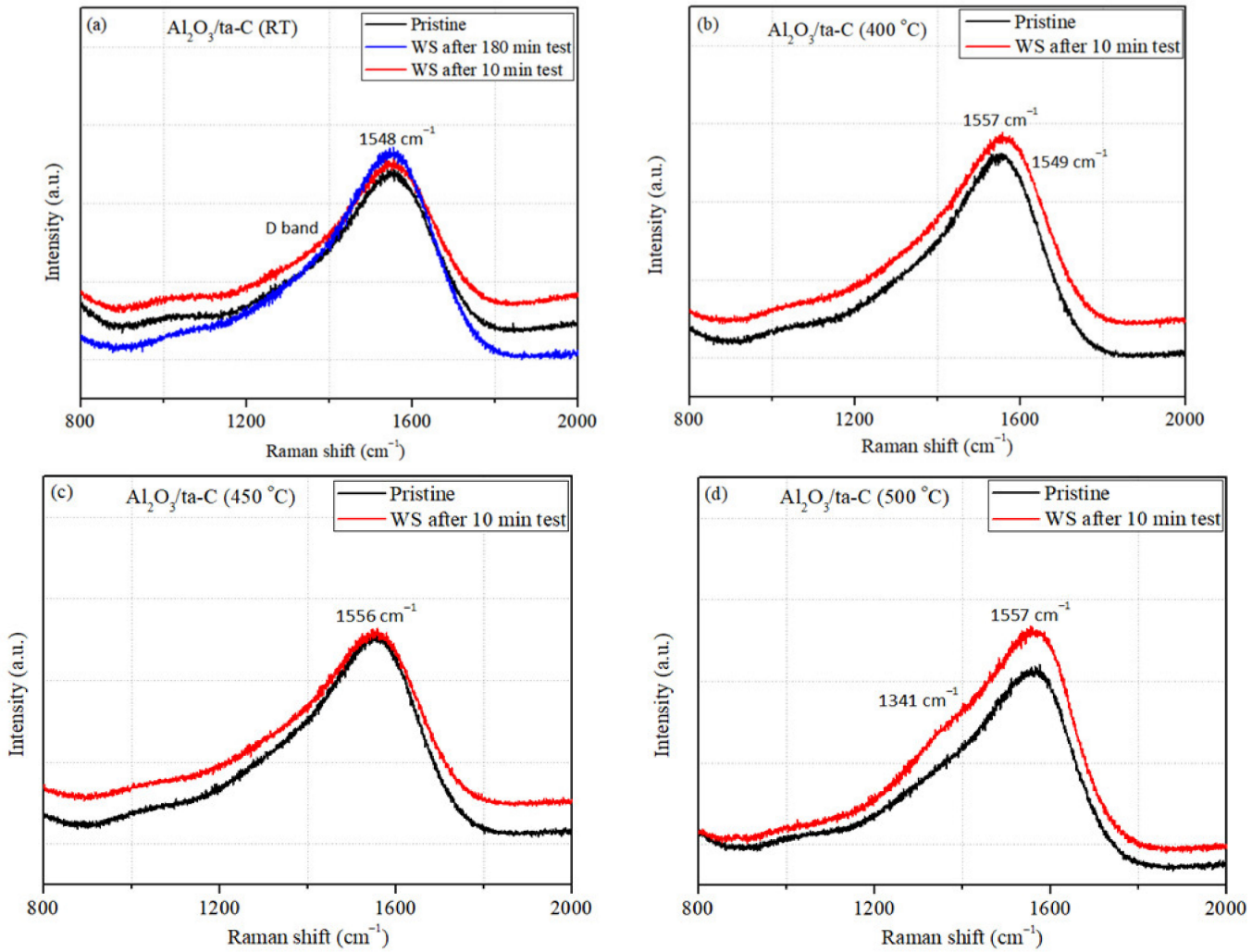

Figure 8. Raman spectra taken on the pristine and within wear scar surfaces of the Al_2O_3/ta-C coating after the sliding tests at (**a**) RT, (**b**) 400 °C, (**c**) 450 °C and (**d**) 500 °C.

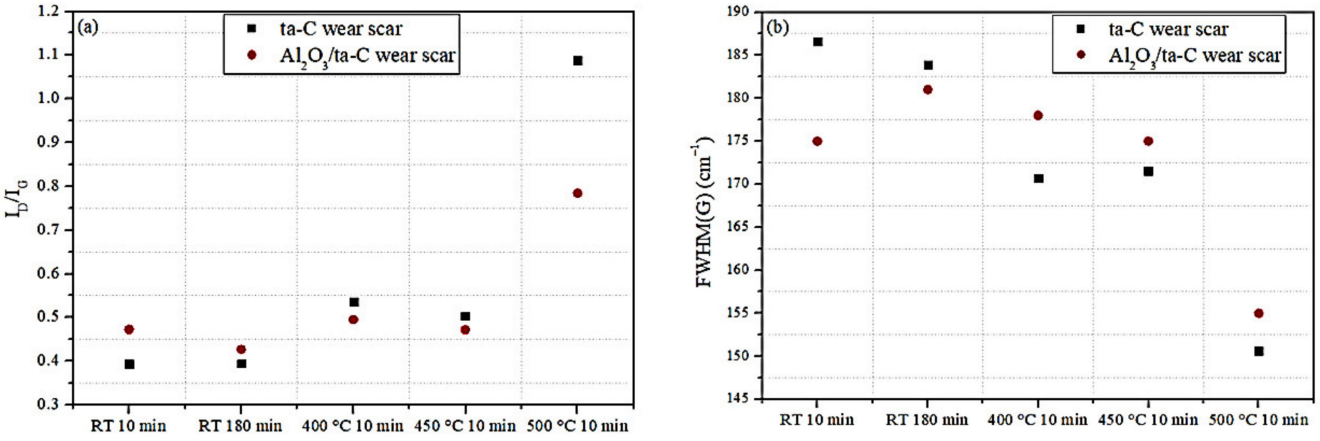

Figure 9. Summary of the results of the Raman spectroscopy investigations within the wear scars: (**a**) I_D/I_G ratio and (**b**) FWHM(G).

To summarize, three studies on the impact of 200 nm thick Al_2O_3 layer prepared on the NCD, a-C:H:Si and ta-C coatings on the tribological performance show an improvement in the oxidation resistance, thermal stability and tribological properties of a wide range of carbon-based coatings tested at HT in ambient air. The adaptation effect was observed, namely the increase of the wear scar width in the sliding tests at RT for coated with alumina carbon-based coatings, which leads to the decrease of contact pressure and wear. The operational temperature for all investigated systems coated with alumina layer can be higher than that of the uncoated surfaces. For instance, in the case of Al_2O_3/ta-C coating, this temperature can be about 50 °C higher than with the ta-C coating.

4. Conclusions

A comparative investigation of the tribological behavior of the ta-C and Al_2O_3/ta-C coatings at elevated temperatures in ambient air was conducted. The alumina layer changes the contact conditions owing to the increased contact area and decreased contact pressure (adaptation effect). The results demonstrate the hereditary effect as well, i.e., the initial contact conditions strongly influence the tribological performance of the coating during extended time tests. The chemical composition of the ta-C layer within the wear scar on Al_2O_3/ta-C differs from that on the ta-C coating after the sliding tests at HT, namely, a higher sp^3 bonds content was observed on the Al_2O_3/ta-C coating, resulting in higher hardness. These results explain the improvement of tribological properties of the Al_2O_3/ta-C coating in comparison with those of the ta-C. The thin alumina layer is a multi-functional layer, which increases the thermal stability, oxidation resistance and durability of the ta-C coating in the sliding tests at HT in air due to the suppression of the atmospheric oxidation.

Author Contributions: Conceptualization, A.A. and V.P.; methodology, A.A. and V.P.; software, A.A., validation, A.B. and A.A., formal analysis, V.P. and A.A., investigation, A.A., T.J., T.R. and M.V., resources, V.P., data curation, A.A., writing—original draft preparation, A.A., writing—review and editing, A.A., V.P., F.S., J.K. (Jakob Kübarsepp), A.L. and J.K. (Jan Kluson), visualization, A.A., supervision, V.P., project administration, V.P., funding acquisition, V.P. and F.S. All authors have read and agreed to the published version of the manuscript.

Funding: This research was funded by the Estonian Ministry of Education and Research under financing projects PUT 1369.

Institutional Review Board Statement: Not applicable.

Informed Consent Statement: Not applicable.

Data Availability Statement: Not applicable.

Conflicts of Interest: The authors declare no conflict of interest.

References

1. Holmberg, K.; Erdemir, A. Influence of tribology on global energy consumption, costs and emissions. *Friction* **2017**, *5*, 263–284. [CrossRef]
2. Ronkainen, H.; Varjus, S.; Koskinen, J.; Holmberg, K. Differentiating the tribological performance of hydrogenated and hydrogen-free DLC coatings. *Wear* **2001**, *249*, 260–266. [CrossRef]
3. Vetter, J. 60 years of DLC coatings: Historical highlights and technical review of cathodic arc processes to synthesize various DLC types, and their evolution for industrial applications. *Surf. Coat. Technol.* **2014**, *257*, 213–240. [CrossRef]
4. Wang, P.; Wang, X.; Chen, Y.; Zhang, G.; Liu, W.; Zhang, J. The effect of applied negative bias voltage on the structure of Ti-doped aC: H films deposited by FCVA. *Appl. Surf. Sci.* **2007**, *253*, 3722–3726. [CrossRef]
5. Yang, L.; Neville, A.; Brown, A.; Ransom, P.; Morina, A. Friction reduction mechanisms in boundary lubricated W-doped DLC coatings. *Tribol. Int.* **2014**, *70*, 26–33. [CrossRef]
6. Charitidis, C.A. Nanomechanical and nanotribological properties of carbon-based thin films: A review. *Int. J. Refract. Met. Hard Mater.* **2010**, *28*, 51–70. [CrossRef]
7. Donnet, C. Recent progress on the tribology of doped diamond-like and carbon alloy coatings: A review. *Surf. Coat. Technol.* **1998**, *100*, 180–186. [CrossRef]
8. Ronkainen, H.; Varjus, S.; Holmberg, K. Tribological performance of different DLC coatings in water-lubricated conditions. *Wear* **2001**, *249*, 267–271. [CrossRef]
9. Flege, S.; Hatada, R.; Ensinger, W.; Baba, K. Properties of hydrogenated DLC films as prepared by a combined method of plasma source ion implantation and unbalanced magnetron sputtering. *J. Mater. Res.* **2012**, *27*, 845–849. [CrossRef]
10. Erdemir, A.; Donnet, C. Tribology of diamond-like carbon films: Recent progress and future prospects. *J. Phys. D Appl. Phys.* **2006**, *39*, R311. [CrossRef]
11. Hainsworth, S.V.; Uhure, N.J. Diamond like carbon coatings for tribology: Production techniques, characterisation methods and applications. *Int. Mater. Mater. Rev.* **2007**, *52*, 153–174. [CrossRef]
12. Tahir, N.A.; Abdollah, M.F.; Tamaldin, N.; Amiruddin, H.; Mohamad Zin, M.R. A brief review on the wear mechanisms and interfaces of carbon based materials. *Compos. Interfaces* **2018**, *25*, 491–513. [CrossRef]
13. Yang, J.F.; Jiang, Y.; Hardell, J.; Prakash, B.; Fang, Q.F. Influence of service temperature on tribological characteristics of self-lubricant coatings: A Review. *Front. Mater. Sci.* **2013**, *7*, 28–39. [CrossRef]
14. Donnet, C.; Fontaine, J.; Le Mogne, T.; Belin, M.; Héau, C.; Terrat, J.P.; Vaux, F.; Pont, G. Diamond-like carbon-based functionally gradient coatings for space tribology. *Surf. Coat. Technol.* **1999**, *120*, 548–554. [CrossRef]
15. Rosenkranz, A.; Costa, H.L.; Baykara, M.Z.; Martini, A. Synergetic effects of surface texturing and solid lubricants to tailor friction and wear—A review. *Tribol. Int.* **2021**, *155*, 106792. [CrossRef]
16. Rouhani, M.; Hong, F.C.; Jeng, Y.R. In-situ thermal stability analysis of amorphous carbon films with different sp^3 content. *Carbon* **2018**, *130*, 401–409. [CrossRef]
17. Grierson, D.S.; Sumant, A.V.; Konicek, A.R.; Friedmann, T.A.; Sullivan, J.P.; Carpick, R.W. Thermal stability and rehybridization of carbon bonding in tetrahedral amorphous carbon. *J. Appl. Phys.* **2010**, *107*, 033523. [CrossRef]
18. Murashima, M.; Deng, X.; Izuoka, H.; Umehara, N.; Kousaka, H. Effect of oxygen on degradation of defects on ta-C coatings deposited by filtered arc deposition. *Surf. Coat. Technol.* **2019**, *362*, 200–207. [CrossRef]
19. Deng, X.; Kousaka, H.; Tokoroyama, T.; Umehara, N. Tribological behavior of tetrahedral amorphous carbon (ta-C) coatings at elevated temperatures. *Tribol. Int.* **2014**, *75*, 98–103. [CrossRef]
20. Bhowmick, S.; Banerji, A.; Khan, M.Z.; Lukitsch, M.J.; Alpas, A.T. High temperature tribological behavior of tetrahedral amorphous carbon (ta-C) and fluorinated ta-C coatings against aluminum alloys. *Surf. Coat. Technol.* **2015**, *284*, 14–25. [CrossRef]
21. Podgursky, V.; Alamgir, A.; Yashin, M.; Jõgiaas, T.; Viljus, M.; Raadik, T.; Danilson, M.; Sergejev, F.; Lümkemann, A.; Kluson, J.; et al. High-Temperature Tribological Performance of Al2O3/aC: H: Si Coating in Ambient Air. *Coatings* **2021**, *11*, 495. [CrossRef]
22. Podgursky, V.; Yashin, M.; Jõgiaas, T.; Viljus, M.; Alamgir, A.; Danilson, M.; Bogatov, A. high temperature tribological properties of Al2O3/NCD films investigated under ambient air conditions. *Coatings* **2020**, *10*, 175. [CrossRef]
23. Alamgir, A.; Bogatov, A.; Yashin, M.; Podgursky, V. Mechanical and tribological properties of 100-nm thick alumina films prepared by atomic layer deposition on Si (100) substrates. *Proc. Est. Acad. Sci.* **2019**, *68*, 126–130. [CrossRef]
24. Veprek, S.; Jílek, M.; Zindulka, O. Method of producing PVD layers using rotary cylindrical cathode and apparatus for making the same. CZ2009784A3, 1 June 2011.
25. Platit. Portfolio. Available online: https://www.platit.com/media/filer/2020/compendium_en61.pdf (accessed on 12 December 2021).
26. Jõgiaas, T.; Zabels, R.; Tamm, A.; Merisalu, M.; Hussainova, I.; Heikkilä, M.; Maendar, H.; Kukli, K.; Ritala, M.; Leskelä, M. Mechanical properties of aluminum, zirconium, hafnium and tantalum oxides and their nanolaminates grown by atomic layer deposition. *Surf. Coat. Technol.* **2015**, *282*, 36–42. [CrossRef]
27. Robertson, J. Diamond-like amorphous carbon. *Mater. Sci. Eng. R Rep.* **2002**, *37*, 129–281. [CrossRef]
28. Ferrari, A.C.; Robertson, J. Interpretation of Raman spectra of disordered and amorphous carbon. *Phys. Rev. B.* **2000**, *61*, 14095. [CrossRef]
29. Tokoroyama, T.; Murashima, M.; Umehara, N. The Surface Enhanced Raman Scattering Analysis for Carbonaceous Coating by Using Au Nano-Particles. *Tribol. Online* **2020**, *15*, 300–308. [CrossRef]

30. Ferrari, A.C.; Robertson, J. Raman spectroscopy of amorphous, nanostructured, diamond–like carbon, and nanodiamond. *Philos. Trans. R. Soc. Lond. Ser. A Math. Phys. Eng. Sci.* **2004**, *362*, 2477–2512. [CrossRef]
31. Mullazzi, E.; Brivio, G.P.; Faulques, E.; Lefrant, S. Experimental and theoretical Raman results in trans polyacetylene. *Solid State Commun.* **1983**, *46*, 851–855. [CrossRef]
32. Donnet, C.; Erdemir, A. (Eds.) *Tribology of Diamond-Like Carbon Films: Fundamentals and Applications*; Springer Science & Business Media: Dordrecht, The Netherlands, 2007.
33. Casiraghi, C.F.; Ferrari, A.C.; Robertson, J. Raman spectroscopy of hydrogenated amorphous carbons. *Phys. Rev. B.* **2005**, *72*, 085401. [CrossRef]
34. Cui, W.G.; Lai, Q.B.; Zhang, L.; Wang, F.M. Quantitative measurements of sp3 content in DLC films with Raman spectroscopy. *Surf. Coat. Technol.* **2010**, *205*, 1995–1999. [CrossRef]
35. Bouchet, M.D.; Matta, C.; Vacher, B.; Le-Mogne, T.; Martin, J.M.; Von Lautz, J.; Ma, T.; Pastewka, L.; Otschik, J.; Gumbsch, P.; et al. Energy filtering transmission electron microscopy and atomistic simulations of tribo-induced hybridization change of nanocrystalline diamond coating. *Carbon* **2015**, *87*, 317–329. [CrossRef]
36. Safaie, P.; Eshaghi, A.; Bakhshi, S.R. Structure and mechanical properties of oxygen doped diamond-like carbon thin films. *Diam. Relat. Mater.* **2016**, *70*, 91–97. [CrossRef]
37. Guo, M.; Diao, D.; Fan, X.; Yang, L.; Yu, L. Scratch behavior of re-structured carbon coating by oxygen plasma etching technology for magnetic disk application. *Surf. Coat. Technol.* **2014**, *251*, 128–134. [CrossRef]